ISSN: 2755-9351

Journal of Alzheimer's Disease & Reports



Research Article Open Access

Functionalized Selenium Nanoparticles with Baicalin-Myricetin with Neuroprotective Effect for Alzheimer's Disease

Rosa Martha Pérez Gutiérrez^{1*}, Julio Téllez Gómez¹, Mónica Corea Téllez², Alethia Muñiz-Ramírez³ and José María Mota Flores¹

¹Natural Products Research Laboratory. Higher School of Chemical Engineering and Extractive Industries. National Polytechnic Institute (IPN) Adolfo López Mateos Professional Unit S/N Av. National Polytechnic Institute Mexico City, Zip Code 07708, Mexico

²Polymer and Nanomaterials Research Laboratory Higher School of Chemical Engineering and Extractive Industries. National Polytechnic Institute (IPN) Adolfo López Mateos Professional Unit S/N Av. National Polytechnic Institute Mexico City, Zip Code 07708, Mexico

³CONAHCYT- IPICYT/Advanced Materials Division. San José Dam Road, Lomas 4th Section, Zip Code 76216 San Luis Potosí, Mexico

ABSTRACT

Background: AD disease involves deposition of $A\beta$ amyloid in the mitochondria of cells, reducing consumption of glucose by neurons reducing enzyme functions. Contemporary drugs therapy for AD are unable to alleviate this disease; since in the short term it only produced symptomatic alleviation, thus is necessary to develop new drugs with curative effects. Objective: To determine the neuroprotective effect of flavonoids combined with selenium nanoparticles (EM@Se).

Methods: Was suc¬cessfully synthesized selenium nanoparticles of Baicalin-Myricetin, characterized using different techniques: UV/vis, Fourier-transform infrared spectroscopy, transmission electron microscopy, DTS, energy dispersive X-ray, vitro drug release, cytotoxicity and in vivo in AD induced by AlCl3.

Results: EM@Se showed optimum particle size (94.52 nm), polydispersity index (0.153), and zeta potential (--30.3 mv) with high entrapment efficiency (88. 7%) NPs achieve significantly maintain EM in vitro release, possesses low cytotoxicity in RAW264.7 macrophage cells. In vivo experiments restore cognitive function to the normal level, reducing hippocampal oxidative damage and decrease A β amyloid in plasma.

Conclusion: This study provides evidence of the neuroprotective effects of flavonoids combined with nanoparticles.

*Corresponding author

Rosa Martha Pérez Gutiérrez, Natural Products Research Laboratory. Higher School of Chemical Engineering and Extractive Industries. National Polytechnic Institute (IPN) Adolfo López Mateos Professional Unit S/N Av. National Polytechnic Institute Mexico City, Zip Code 07708, Mexico.

Received: February 13, 2025; Accepted: March 03, 2025; Published: June 28, 2025

Keywords: Alzheimer's Disease, Baicalin, Myricetin, Selenium Nanoparticles

Introduction

Alzheimer's disease (AD) is associated with protein aggregation and is a factor cause of behaviorals, neurodegenerative diseases, enhanced cytotoxicity and amyloid diseases [1]. In AD, the aggregating proteins in the form of neurofibrillary tangles intervene in neurotoxicity, formed by hyperphosphorylated tau and extracellular senile plaques placed in small peptides of amyloid- β (A β) derived from sequential proteolytic cleavages of the amyloid precursor protein (APP) [1-3].

The production of aggregation-prone A β species is facilitated by intense changes in APP metabolism; these mutations form the basis for the "amyloid cascade hypothesis" in AD pathogenesis [3].

Alzheimer's (AD) is a neurodegenerative disease associated with a progressive cognitive decrease [4]. Among, pathological

mechanisms microtubule-associated protein, amyloid β (A β) inhibition of AChE and butylcholines are three important parameters contribute to the initiation and progression of the Alzheimer's disease which is associated with different mechanisms such as a decrease in specific neurotransmitters, synaptic loss, neuroinflammation and neuronal death [5]. Thus, the AD-target produces less improvement than those in multiple targets [6]. Butyrylcholinesterase (BuChE) is a serine hydrolase that catalyzes the hydrolysis of non-choline esters, the neurotransmitters acetylcholine and choline. BuChE partic- 63 ipates in neural function consequently it is widely distributed in the nervous system. In addition, it plays an important role in cholinergic neurotransmission and neurodegenerative diseases [7].

Also, AD is characterized by intracellular neurofibrillary tangles (NFTs) formed by au aggregates and the deposition of extracellular $A\beta$ plaques. Tau is a microtubule- related protein stabilizing neuronal microtubules in normal physiological conditions. Meanwhile, in pathological circumstances, tau protein is altered

J Alzheimers Dise & Rep 2025 Volume 2(1): 1-13

via phosphorylation-generated aggregates that are toxic to neurons. This procedure is known as tauopathies found in neurological disorders [8]. In the progression of AD, hyperphosphorylation of tau interrupts the association of tau with MTs and induces tau aggregation in neurons [9]. β -amyloid (A β) peptide, which is found in extracellular senile plaque cores, is derived from the transmembrane amyloid precursor protein and plays an important role in the neurodegeneration in later stages of AD.

Memory ability, cognitive disorders, and impaired memory and learning are always associated with neurodegenerative diseases like AD. In AD, cognitive impairment is related to a synaptic disability in the cholinergic system, caused by an insufficiency of ACh induced to augment the level of AChE in the brain [10]. The loss of plasticity is the main symptoms of AD, which have an important effect on dendritic ramifications in processes such as synaptogenesis, neurogenesis, axonal sprouting, neurite extension, long-term potentiation (LTP), and synaptic remodeling. Unfortunately, medical compounds are not working in decremental LTP and memory dysfunction [11,12]. Modification in protein architecture produces abnormalities and an accumulation of mis folded proteins, which in turn produces human diseases, including Parkinson's disease, Alzheimer's and type II diabetes, which are characterized by the accumulation of amyloid aggregates that alter protein structure and dynamics. These adducts accumulate in the brain through aging [13]. In AD patients, the presence of microglial cells, Aß deposition and increased AGE levels possess a pathological role in this neurodegeneration disease [13]. To date, several potential therapies, including tau-targeting, β-amyloid (Aβ)-targeting, and immunotherapies, used in clinical trials for AD have shown side effects and poor effectiveness [14].

In nature, selenium compounds exist in four oxidation states: elemental selenium (Se0), selenide (Se2–), selenite (Se4+), and selenate (Se6+). Only Se0 is non-toxic and soluble in water [15]. Considering the various oxidation states of selenium, toxicity can be reduced through nanosizing. Different selenium oxidation states' toxic responses are linked to their aqueous solubility and bioavailability. Selenium also exists in various chemical forms, including organic selenium compounds like selenium-methyl-selenocysteine, selenocysteine, and selenomethionine, as well as inorganic forms like selenate and selenite. Selenium nanoparticles (SeNPs) exhibit significantly lower toxicity and enhance selenoprotein activities than other selenium forms [16].

SeNPs can be used as therapeutic agents for various diseases, including liver injury antimicrobial resistance, diabetes, and Alzheimer's disease, due to their ability to enhance drug delivery by selectively targeting healthy and diseased cells. This targeted release reduces side effects and ensures delivery to specific tissues [17]. Another essential feature of SeNPs is their ability to mitigate drug-induced toxicity. For instance, polyacrylic acid-coated selenium-doped carbon dots (SeCD) significantly enhance cisplatin's anti-tumor activity and improve biocompatibility [18].

SeNP toxicity is associated with membrane disruption and increased ROS generation [19]. Experiments with zebrafish, which share 85% of the human genome, show that SeNPs at lower concentrations (5–10 $\mu g/mL)$ do not cause significant mortality [20]. However, higher concentrations (20–25 $\mu g/mL)$ lead to notable abnormalities and mortality. In another study with rat dermal fibroblasts, the half maximal inhibitory concentration (IC50) of 46.5 $\mu g/mL$ measures the potency of a substance in inhibiting a specific biological function. However, concentrations below 31 $\mu g/mL$ increased the number of live cells, indicating

that selenium nanoparticles can be toxic or benign depending on the dose [21]. Lower concentrations of SeNPs are metabolized in the liver and kidneys. Exposure to higher concentrations of SeNPs leads to the formation of selenopersulfide intermediates, causing toxicity and oxidative [22]. Assuming that Se nanoparticles may cause minimal adverse effects, flavonoids can mitigate these effects due to their ability to interact with SeNPs through OH groups on their rings, enhancing the protective effect of flavonoids. The combination of flavonoids and nanoparticles improves the interfaces and surfaces in drug delivery systems [23]. However, Myricetin and Baicalin possess low water solubility, considered as a main challenges in drug absorption. Thus, one possible strategy for flavonoids delivery is loaded it's in to other water-soluble material. When solubility is modified using nanoparticles as SeNPs the new nanoparticle possesses high water solubility.

Based on the improved effects of selenium nanoparticles (Se NPs) over selenium (Se), have been investigated in of selenium nanoparticles (Se NPs) over selenium (Se), have been investigated in several disease conditions. Nanoparticles ameliorate bioavailability with the advantage of reduced toxicity. The antioxidant and prooxidant properties have been studied in different pathological conditions and are capable of free radical scavenging both in studies in vivo and in vitro. Consequent could be used as anti-oxidative drugs [24]. In addition, Se participates in the normal physiological functions of the brain with a neuroprotective activity; also, Se avoids the damage produced by oxidative stress [25].

Investigation on polyphenols indicates that these have the ability to decrease AD involving the inhibition of inflammation, oxidative stress, β-secretase, Tau protein aggregation, butyrylcholinesterase, acetylcholinesterase, and apoptosis through modulation of signaling pathways including MAPKs, NFKB, PI3-kinase/Akt, and ERK [26]. Baicalin improved memory impairment in the Morris water maze test, reduced glial cell activations and increase of IL-6 and TNF-α expressions produced anti-neuroinflammatory effect [27]. Baicalin increased the number of astrocytes and neuronal cells and enhanced the expressions of NSE and Nestin [28]. Myricetin (M) can significantly enhance memory and learning abilities in animal model of Alzheimer's disease [28]. Also, can form stable semiquinone radicals when combine with radicals, thus preventing the radical chain reaction, regulates autophagy through the mTOR pathway by reducing mTOR's phosphorylation, including PI3K/ PDK 1/Akt, pathways ERK1/2 and AMPK-PGC-1αSirt3 [29,30]. Inhibit the activity of BACE-1 and hinders the production of Aβ, reduced the impairment of memory and learning ability of mice through its AChE inhibitory effect [31]. For several decades many therapeutic strategies have been examined, unfortunately treatments currently are therapies of symptoms [32].

In this investigation, we combined Baicalin-Myricetin (EM) into selenium nanoparticles (Se-EM) to ameliorate the low bioavailability of EM and promote the neuroprotective effects. Toxicological, behavioral, and biochemical, evaluation was investigated in induced-AlCl3 in mice model neurodegenerative diseases.

Materials and Methods Chemicals and Material

Bovine serum albumin (BSA, Sigma Aldrich, Saint Louis, MO); Aluminum trichloride (AlCl3, Sigma Aldrich, Saint Louis, MO); ascorbic acid (Sigma Aldrich, Saint Louis, MO); selenous acid (Sigma Aldrich, Saint Louis, MO); Baicalin (BiocSciences, On, CAN); Myricetin (BiocSciences, On, CAN); ammonium

bicarbonate (Thermo Fisher CDMX); magnesium chloride hexahydrate ((Themo Fisher CDMX); sodium chloride ((Themo Fisher CDMX); sodium bicarbonate (Merck, CDMX); potassium dihydrogen phosphate (Sigma Aldrich, Saint Louis, MO); (pH 3.0) or simulated intestinal fluid (SIF, pancreatin (Haiyang Industry, Shandong China); bile salts (Shandong Province, China); magnesium chloride hexahydrate (Haiyang Shandong Province, China); potassium chloride (Themo Fisher CDMX); Acetylcholinesterase (Sigma Aldrich, Saint Louis, MO); butyryl thiochline (Sigma Aldrich, Saint Louis, MO); Thioflavin T (Merck, CDMX); Congo red (Merck, CDMX).

Selenium Nanoparticle Synthesis

Bovine serum albumin-coated selenium nanoparticles (Se NPs) using a one-step reaction involving selenous acid (H2SeO₃), ascorbic acid, and BSA. To prevent nanoparticle aggregation, BSA was added for stabilization, leveraging its biocompatibility with selenium, while ascorbic acid served as the reducing agent. Specifically, we gradually added 50 mM ascorbic acid dropwise to a 1 mL aqueous solution containing H2SeO₃ (100 mM) and BSA (10 mg/mL). As the reductant mixed with selenous acid, the solution turned light yellow and eventually dark red. After 120 minutes of reaction time, we collected the nanoparticles via centrifugation (20 minutes for 18,000 rpm) and washed them with H2O and Milli-Q [33].

Synthesis of EM/Se@BSA NPs

To synthesize nanoballs (EM/Se@BSA NPs), we combined selenium nanoparticles (Se NPs) with a mixture of Baicalin and Myricetin (25 mM) dissolved in a 1:1 ethanol-water solution (100 mM Se NPs). The reaction was gently shaken for 1 hour for analysis and then collected by centrifugation (16,000 rpm for 10 minutes). The precipitate was washed with Milli-Q water and the supernatant was removed. This process was repeated three times to ensure the removal of any other compounds. Finally, the solution containing nanoballs was dialyzed for 24 hours with Milli-Q water for 24 hours, being stored at room temperature [34].

Characterization of Se NPs and EM/Se@BSA Nanoparticles

The size and polydispersity (PDI) of the nanoparticles using dynamic light scattering (DLS). Additionally, we measured the Zeta potential of Se@BSA NPs and EM/Se@BSA NPs using a Zetasizer Nano ZSP (Malvern Instruments, Malvern, UK). These measure ments were performed in triplicate at 25°C. For surface morphology analysis, we employed a high-resolution transmission electron microscope (TEM; Model HT7700, Hitachi High-Tech, Tokyo, Japan). The infrared spectrum of the nanoparticles was obtained using a Bruker FTIR-TENSOR27 spectrophotometer (Ettinger, Germany) in the range of 400–4000 cm⁻¹. Furthermore, UV-visible spectra were acquired using a Shimadzu UV-1800 spectrophotometer in Tokyo, Japan. Finally, X-ray photoelectron spectroscopy (XPS) was conducted using a spectrometer equipped with a monochromatic Al Kα x-ray source (Thermo-Fisher ESCALAB 250xi).

UV-vis spectrophotometer

The reduction of Se ions in the reaction mixture using an aliquot of 1 mL of nanoparticles at three different concentrations (8, 10, and 12 μ g/mL). UV-visible spectrophotometer measurements were taken at 30-minute intervals, with the wavelength set between 200 and 600 nm. Milli-Q water served as the blank control [26].

Fourier Transform Infrared Spectroscopy

The Fourier transform infrared (FTIR) spectrum revealed potential biomolecules responsible for synthesizing and stabilizing Se nanoballs, as well as functional groups pre-sent on the nanoparticle surface that may play a role in sorption processes. For analysis, dried nanoparticle samples (2 mg) were used, and the FTIR scan covered a range between 1000 and 3500 cm⁻¹ [35].

Transmission Electron Microscope (TEM)

To evaluate the morphology of selenium nanoparticles (SE NPs), transmission electron microscopy (TEM) at 200 kV was used. The solution was diluted with deionized water and subsequently sonicated (Vibronics VS 80) for 10 minutes. To obtain the electron micrographs, 2 mg of the sample were placed on copper grids which were covered with carbon, drying the sample under vacuum for 30 minutes [35].

Dynamic Light Scattering Spectroscopy

To analyze how the size of the particles was distributed in the sample, 3 mg of nanoparticles were analyzed by dynamic light scattering (DLS) at a temperature of 25°C, using laser attenuation filters that were automatically adjusted. This analysis provided us with information about the polydispersity index (PDI) and the size of the nanoballs. Particle size was reported as mean \pm standard deviation [35].

Energy Dispersive X-ray Study

To confirm whether the selenium ions were converted to elemental selenium, energy dispersive X-ray (EDX) assay was performed. 1 mg of sample was prepared in the same way as for TEM. Subsequently, the TEM micrograph was analyzed using EDX. The percentage of metal atoms obtained in the EDX analysis helped us determine the elemental composition and purity of the nanoparticles [35].

Encapsulation Efficiency (EE, %) and Loading Capacity (LC, %) of EM in Se@BSA

EM-loaded Se@BSA nanoparticles were prepared following the previous study. Specifically, EM-loaded Se@BSA nanoparticles (40 mg) were dispersed in MeOH and stirred for 3 h at 600 rpm. Subsequently, the mixture was centrifuged, for 1 hour at 10000 \times g [36]. The concentration of non-encapsulated flavonoids was determined in the supernatant using a UV-1800 spectrophotometer (Shimadzu Corporation, Kyoto, Japan) at 271.5 nm. The encapsulation efficiency (EE, %) and drug loading capacity (LC, %) of EM were calculated using the following equations:

Encapsulation efficiency EE (%) =
$$\frac{Amount\ of\ encapsulated\ EM}{The\ total\ amount\ of\ EM} \times 100\%$$
 (1)

Loading capacity (LC%) =
$$\frac{Amount total EM entrapped}{The total Selenium NPs weight} \times 100\%$$
 (2)

In Vitro Flavonoids Release Studies

EM/Se@BSA nanoparticles (200 mg) were dispersed in 25 mL of simulated gastric fluid (SGF, pH 3.0) containing 8.0 g/L pepsin, 0.02 g/L ammonium bicarbonate, 0.01 g/L magnesium chloride hexahydrate, 1.38 g/L sodium chloride, 1.05 g/L sodium bicarbonate, and 0.06 g/L potassium dihydrogen phosphate. Alternatively, the nanoparticles were dispersed in simulated intestinal fluid (SIF, pH 7.0) containing 2.5 g/L pancreatin, 6.3 g/L bile salts, 0.03 g/L magnesium chloride hexahydrate, 1.12 g/L sodium chloride, 3.75 g/L sodium bicarbonate, 0.05 g/L potassium dihydrogen phosphate, and 0.25 g/L potassium chloride. The mixture was divided into equal volumes and placed in separate Eppendorf tubes [36]. Subsequently, the tubes were incubated at 100 rpm/min at 37°C. Every 0, 0.5, 1, 2, 3, 4, 5, 6, 7, and 8 hours, a tube was removed from which the EM was extracted in BSA-Se NPs with ethanol and the sample was subsequently read at 360 nm in a spectrophotometer. The percentage of cumulative release

was calculated with the following equation:

Cumulative release % = released EM \times 100/total EM (3)

Cytotoxicity of EM/Se@BSA NPs

To evaluate the cytotoxicity of the EM/Se@BSA and Se@BSA NPs, the 3-(4,5-dimethylthiazol-2-yl)-2,5-diphenyltetrazolium bromide (MTT) assay was used normal RAW264.7 macrophage cells from Sigma, St Louis, MO, USA. Cells (5 × 104 cell/well) were seeded in Dulbecco's modified eagle's medium (DMEM; Gibco) containing 100 U/mL penicillin, 100 µg/mL streptomycin, and 10% fetal bovine serum The above was incubated in in a 96 well plate with 5% CO2 at 37 °C for 24 h to reach a cell density of 80% confluence, the cells were treated with different concentrations of nanoparticles (0, 18.7, 37.5, 75, 150, 300 and 400 μg/mL). The different concentrations used were chosen considering previous research where Se NPs were analyzed [37]. Untreated cells were used as a negative control and the cells with solvent were the cells that were treated with 5% DMSO. After the incubation time (24 h), 20 µL of MTT dye (5 mg/mL) was taken and added to all wells, including the wells containing untreated cells, the plate was incubated again for 4 h. Subsequently, to dissolve the formazan crystals, the medium was aspirated and DMSO (100 µL) was added to all wells. The samples were read in a microplate reader at 570 nm.

Experimental Protocol

Six groups (n = 6) were established and subjected to various treatments. Aluminum chloride (AlCl₃) solution was prepared by dissolving AlCl3 salt in Milli-Q water adjusted with phosphate-buffered saline (PBS; pH 7.4). This stock solution was used to achieve a dose equivalent to 100 mg/kg of AlCl₃ [38]. The choice of this dose was based on previously published research. The treatment groups were as follows: Group I (normal), Group II (AlCl₃ treatment at 100 mg/kg) administered orally once daily for 7 weeks, Group IV (AlCl₃ + 30 mg/kg of Se@BSA nanoparticles), Group V (AlCl₃ + 30 mg/kg of EM), Group VI (AlCl₃ + 30 mg/kg of EM/Se@BSA nanoparticles), and Group VII (AlCl₃ + 30 mg/kg of Gonepezil). Samples were administered daily via nasal administration. Treatment with all samples continued for seven weeks.

T-maze Test

The T-maze test evaluates spatial learning and memory according to already established protocols [39]. The T-maze test consists of two tests performed at 1-hour intervals. In the first trial the animals were allowed to explore only the familiar arm of the T-maze and the initial arm, while the third arm containing food remained blocked. In the second trial, animals were placed in the initial arm allowing them to explore the three arms freely for 5 minutes. The total time in the third arm was recorded using a camera placed on the ceiling of the maze, to later analyze the images.

Novel Objection Recognition (NOR) Test

This test evaluates the rodents' spontaneous preference for interacting with a novel object rather than a familiar one. In the habituation phase which was carried out for 5 minutes one day before the experiment, the animals were allowed to freely explore an empty arena (50 cm \times 50 cm \times 25 cm). Subsequently, two identical objects which matched in size, shape, color and texture were placed in the sand, allowing the animals to explore them for 10 minutes. During the experimental phase, one of the objects was

replaced with a new one, repeating the procedure for another 10 minutes. The total drainage time in the third arm was recorded using a camera located on the ceiling for subsequent analysis [39].

Exploratory Behavior in Open-Field Test

Through the open field test, exploration behavior is evaluated using already established protocols [40]. The animals were placed in the center of the arena allowing them to explore freely for 5 minutes. On the day of the test, the animals were placed in the center of the box, observing and recording their trajectory and the time spent exploring the center of the arena in 5 minutes. The behavior of the animals is recorded with a video camera. The open field was cleaned with 70% alcohol to reduce olfactory signals between each test. To quantify locomotor behavior, the total number of crossed squares is counted [41].

Biochemical Parameters

24 hours after the last behavioral experiment, the mice were sacrificed by decapitation. Blood was centrifuged at 3,000× g for 15 minutes. The serum was used for determination of amyloid aggregates (A β 1–42) levels. While hippocampal was homog¬enized with ice-cold phosphate-buffered saline solution (pH 7.2) and a protease inhibitor cock¬tail. After was centrifuged at 10,000× g for 15 minutes at 4°C. Then glutathione, CAT, SOD, NO and MDA were evaluated in the supernatant using Abcam assay kits (MA, USA) according to the manufacturer's protocol [41].

ELISA Detection of Amyloid Aggregates in Plasma

 $A\beta1$ –42 levels in plasma were tested after treatment of nanoparticles 7 weeks of nanoparticle treatment using a sensitive sandwich ELISA kit (Wako Chemicals, Richmond, VA) according to the manufacturer's instructions. The data were recorded at 450 nm using a microplate reader (Biorad, USA).

Statistical Analysis

All values were reported as mean \pm standard deviation (SD). Statistical analysis used Student's t-test to compare two groups for continuous variables with normal distributions. For multiple groups, a one-way analysis of variance (ANOVA) was used, followed by Tukey's post hoc analysis. p-values less than 0.05 were considered statistically significant.

Results

Characterization of EM/Se@BSA NPs UV/Vis Spectrophotometer In Figure 1A, the chemical structures of compounds E and M are shown. Initially, the color of the reaction was pale yellow, gradually transitioning to intense red (Figure 1B). This color change is associated with the excitation of surface plasmons in selenium (Se) nanoparticles, indicating the reduction of H2SeO3 to Se nanoparticles. Figure 1B also illustrates that Se nanoparticles remained stable in water for 170 days, exhibiting a transparent appearance suggestive of nanoparticle formation. UV-visible spectrophotometry revealed the absorption of EM at 271, 319, 437 nm (Figure 1C). Figure 1D showed a characteristic absorption peak at 267.5 nm due to the surface plasmon of Se in Se@BSA; a characteristic absorption peak at 266.5 nm, confirming the formation of EM/Se@BSA (Figure 1E). The UV spectra centered at 266.5 nm further support successful EM solution absorption onto the nanoparticle surface (Figure 1E). Stability was monitored using Zeta sizer readings (Data not shown).

J Alzheimers Dise & Rep, 2025 Volume 2(1): 4-13

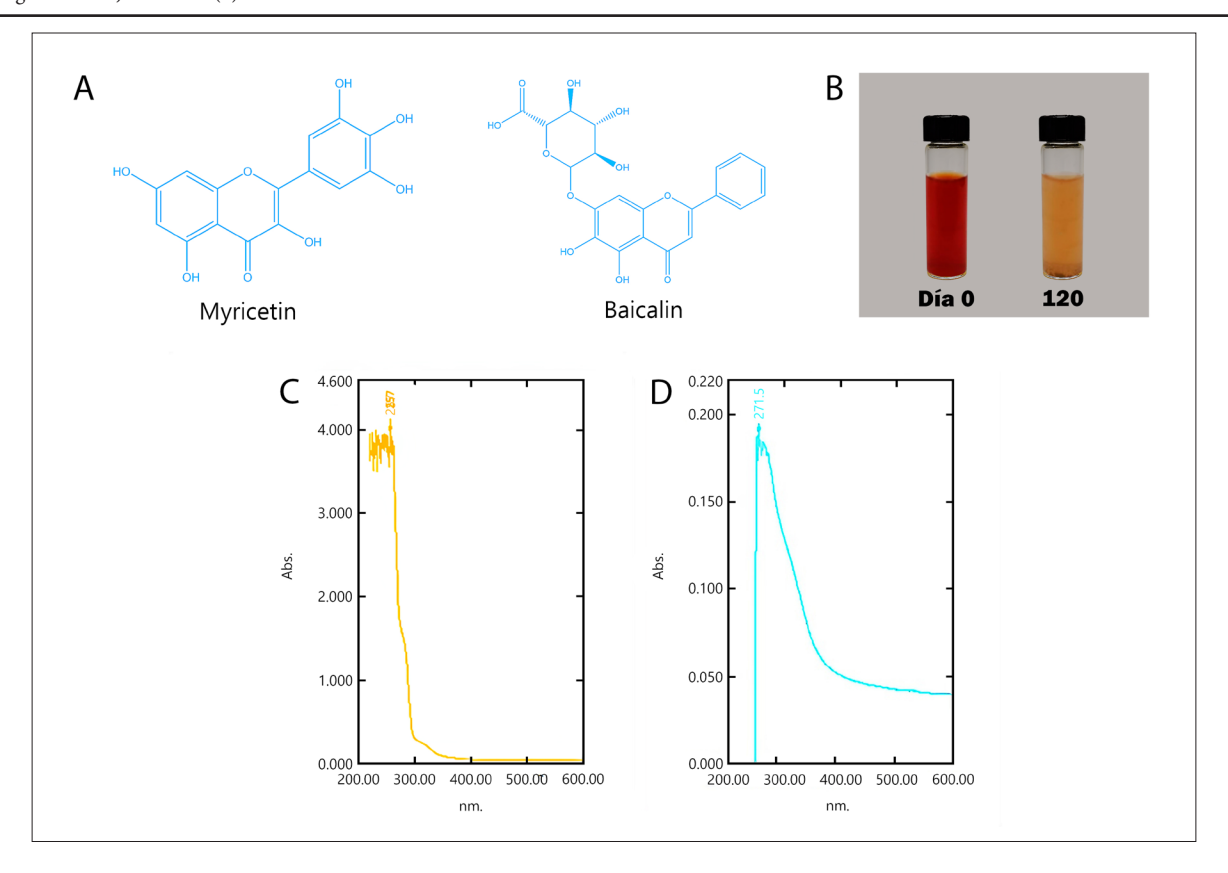


Figure 1: The Chemical Structure of Baicalin and Myricetin (A); Stability for 170 days (B); UV–Visible Spectra EM (C); Se@BSA (D); EM/Se@BSA (E), n=3.

Intermolecular Interaction

Results obtained using FTIR spectroscopy investigate the intermolecular interaction between flavonoids and nanoparticles (Figure 2). The measurements were registered in a range from 400 to 4000cm⁻¹. The EM presents the following peaks: hydroxyl 3267cm⁻¹, carbonyl at 1756 cmcm⁻¹, and groups. 2925, 1656, 1594, 1517, 1462,1376, 1335, 1298, 1199, 1181, 1167, 1084, 1027, 830 and 722 cm⁻¹. The peak at 3267 cmcm⁻¹ indicates the presence to -OH stretching; the peak at 2925 cm⁻¹ s stretching to CH2 and C-H stretching of aliphatic groups; 1534cmcm⁻¹ associated to C=O stretching; 1517cm⁻¹ to aromatic C=C stretching vibraion; 1594 cm⁻¹ associated to C=C stretch of benzene ring; CH2 bond is related with the stretching vibrations at 1335 cm⁻¹; 1199 cm⁻¹ and 1027cm⁻¹ at -C-O stretch. Among them, absorptions in 1756, 1656, 1462, and 1335 cm⁻¹ are characteristics of flavonoids (Figure 2). In this study, we used the FT-IR spectrum to try to describe the interactions between EM and Se@BSA better to form EM/Se@BSA nanospheres. In Se@BSA showing a strong hydrogen bonding interaction (Se–O–H) between the O–H groups of the water at 3310 cm⁻¹ corresponds to H-O-H deformational vibrations. Picks in 1750, 1647, 1635, 1350 and 1156 cm⁻¹ indicate la formation of selenium nanoparticles with BSA. In EM/Se@BSA the appearance of the peaks at 1623, 1 1553, 1445, 1442, 1303, 1249. 1199 and 1143 cm⁻¹ suggest that several -OH groups of EM are conjugated with selenium, producing a perturbation to the hydrogen bonding in native EM and generation of new C-O···Se bonds. EM spectrum was very different from Se@BSA, demonstrating that EM is not only associated with Se@BSA. Rather, they are found strongly attached to the surface of Se and stabilized nanoparticles. FTIR fingerprint analysis has a strong specificity, and a great quantity of information on the main functional groups of bioactive constituents in medicinal plants. Each chemical compound has their own infrared characteristic bands, consequently the difference in absorption shown in Se@BSA, EM and EM/Se@BSA spectrograms reflect the dissimilarity among them confirming the formation of EM/Se@ BSA.

J Alzheimers Dise & Rep, 2025 Volume 2(1): 5-13

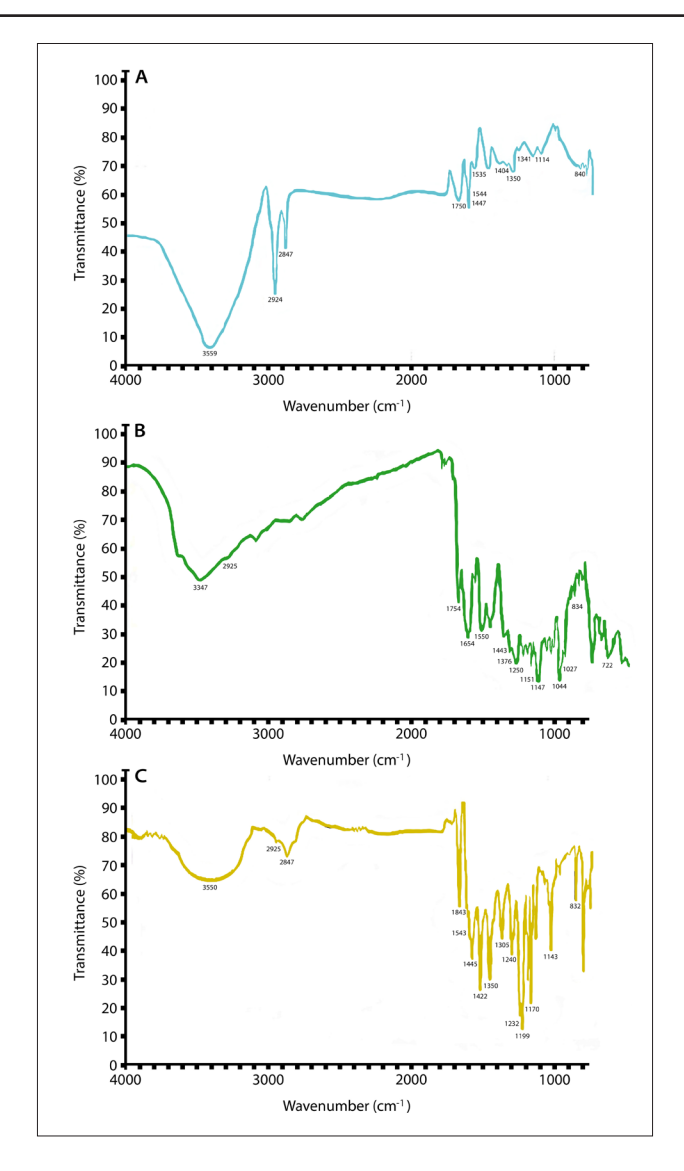


Figure 2: FT-IR Spectra: Se NPs (A); EM (B); EM@Se (C).

Particle Size Distribution

Red elemental selenium was synthesized by reducing bulk selenium to its nanoscale form. Dynamic light scattering (DLS) was used to measure the average particle size, polydispersity index (PDI), and zeta potential of both selenium nanoparticles Se@BSA and EM/Se@BSA (Figure 3A-D). The findings indicated that EM/Se@BSA had an average size of 94.52 nm, a zeta potential of -30.3 mV, and a PDI of 0.153 (as shown in Figure 3). The negatively charged nanoparticles supported their stability. Additionally, DLS analysis of the colloidal dispersion containing selenium nanoparticles indicated an average size of 90.57 nm, a zeta potential of -27.2 mV, and a PDI of 0.270 for EM-loaded nanoparticles, revealing a homogeneous size population in the aqueous medium. These DLS results were consistent with TEM data.

J Alzheimers Dise & Rep, 2025 Volume 2(1): 6-13

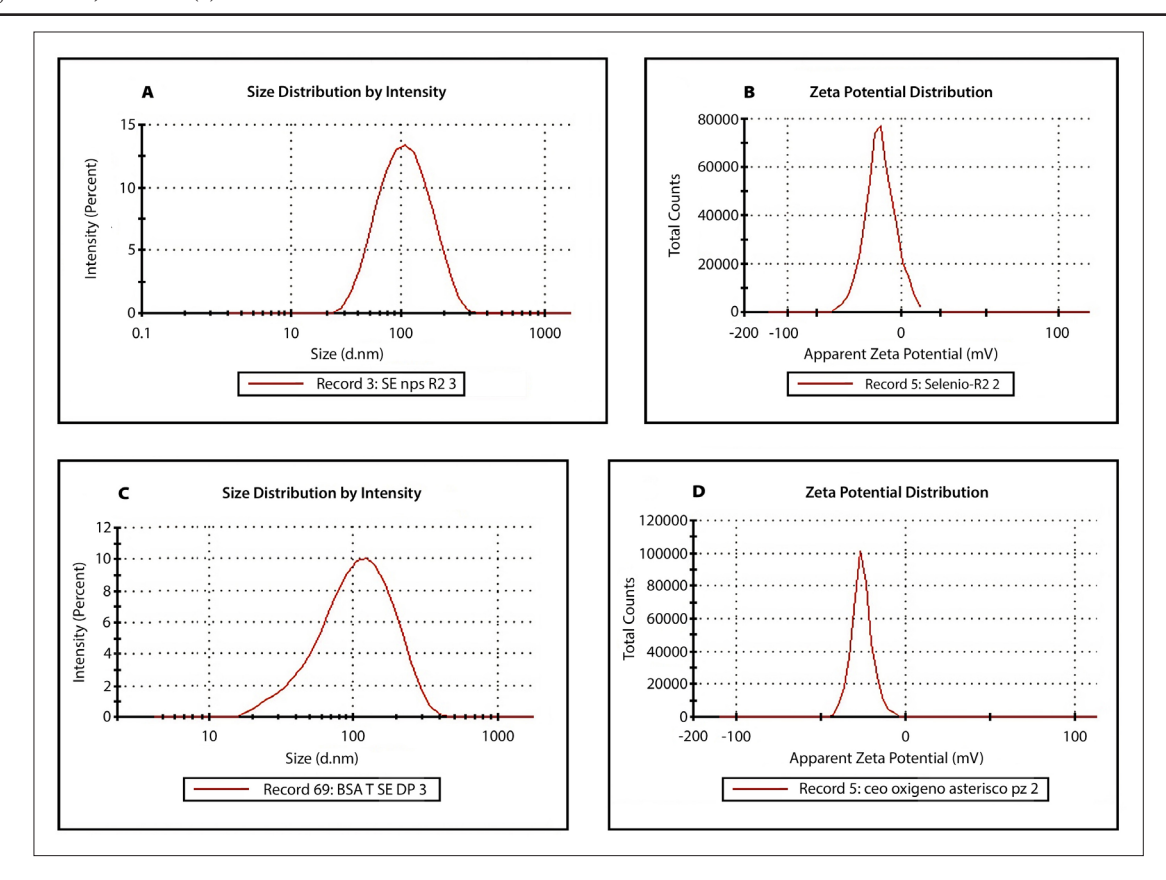


Figure 3: Measurements of Total Counts (u.a) as a Function of Zeta Potential (mV). Size Distribution and Zeta Potential of Se NPs (A); Size Distribution and Zeta Potential of EM@Se (B).

Transmission Electron Microscopy

Scanning Electron Microscopy, The high-resolution TEM image of Se@ BSA nanoparticles revealed a spherical shape (Figure 4A), while the morphology of EM/Se@BSA is mostly spherical in shape and with-out agglomeration (Figure 4B). TEM image revealed a significant difference in chemical composition among the Se NPs untreated and loaded with the flavonoids.

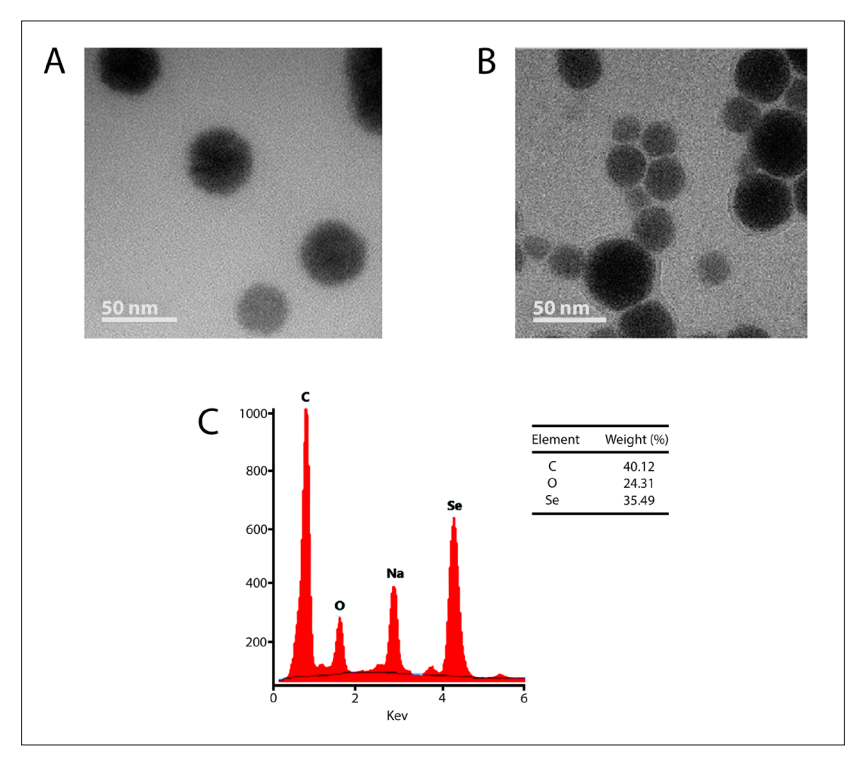


Figure 4: Images of Synthesized Nanoparticles: (A) Se NPs NPs (50 nm); (B) EM@Se (50 nm); X-Ray Diffraction Pattern of Synthesized; (C) Se NPs NPs; (D) EM@Se.

J Alzheimers Dise & Rep, 2025 Volume 2(1): 7-13

X-Ray Diffraction (XRD) Analysis of EM/Se@BSA

The XRD spectrum (Figure 4C) of the biosynthesized BSa/SeNPs has presented an intense peak at 1.5 keV signifying the entire composition of Se in the developed Se Nanoparticles. Figure 4D represents the analysis of X-ray diffraction of the crystal structure of EM/Se@BSA with their characteristic peaks derived from their elemental composition. Different peaks of elements, such as C, O, Na, and selenium, were detected. The elemental analysis indicates the peak of selenium. The elemental analysis indicates the peak of selenium around 24.25% of mass confirming transition from bulk form to nano form. The pure crystalline phase of /Se@BSA is revealed by the clarity of the signals. The element found in the greatest quantity is carbon (40.12%), followed by selenium with 35.49 % and 24.31 % for oxygen (w/w).

Encapsulation Efficiency (EE, %) and Loading Capacity (LC, %) of EM in EM/Se@BSA

The percentage of the EM entrapped in selenium NPs is known as encapsulation efficiency is associated to the ratio between EM and Se@BSA which differs in the solubility of EM in the matrix material. In our investigation, the EE was obtained in 88.7% (1:0.5), 79.8% (1:0.75) and 69.2% (1:1), (Figure 5A). In selenium/EM ratio of 1:0.5 was obtained the highest efficiency. The efficiency markedly is improved as diminish the weight ratio between selenium/EM this is produced by for the increase of saturation of EM cannot be adsorbed by Se@BSA and compounds are rapidly released during the centrifuge. Loading capacity (LC) refers to the quantity of EM encapsulated per unit weight of Se NPs and is significantly influenced by the molecular weight of the compounds being encapsulated. This results in a reduced loading capacity of the Se NPs, which ranges from 51.2% (1:0.5), 39.4% (1:0.75), to 29.1% (1:1) (Figure 5A). The results indicate that EM/Se@BSA has an excellent delivery capacity.

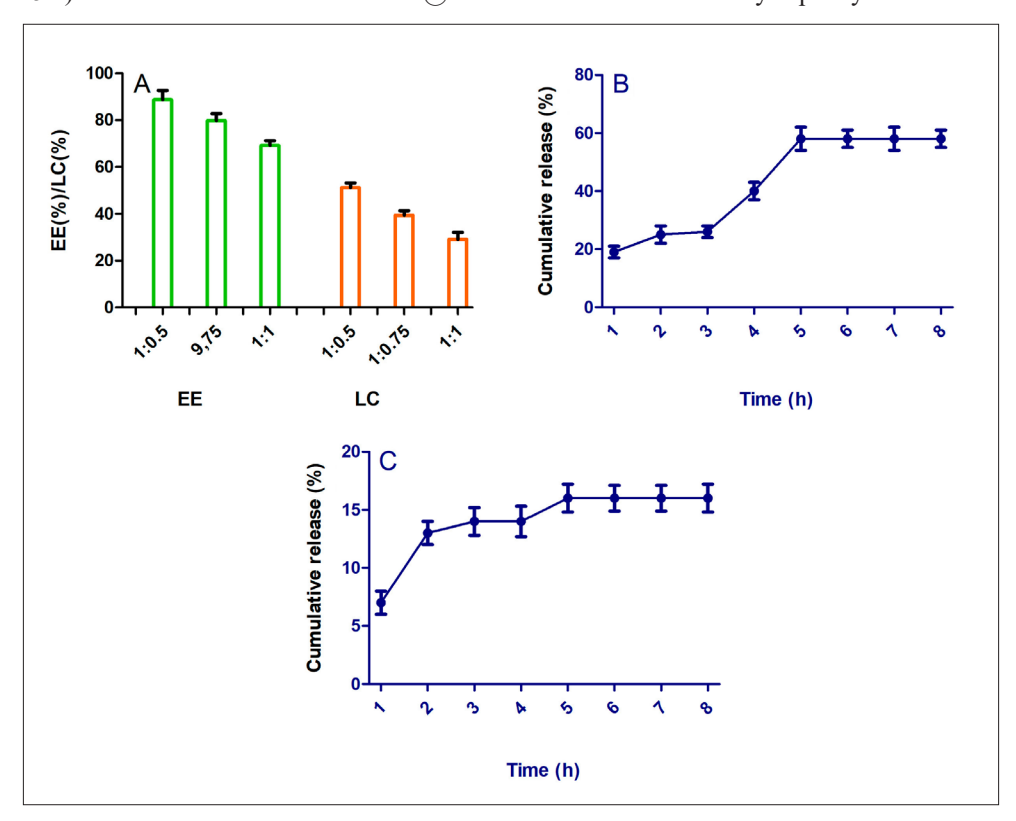


Figure 5: Encapsulation Efficiency (A); Loading capacity at ratio of 1:0.5, .075, and 1:1 of selenium/EM; (A) The cumulative release rate of EM in the EM/Se@BSA. Release during simulating gastric (B) and intestinal digestion processes (C). n=3.

In Vitro Sustained Release of EM

In vitro release profiles of IEM from nanoparticles placed in simulated gastric fluid (pH 3.0) and intestinal fluid (pH 7.0) are shown in Figure 5. Drug release of EM is controlled by pH during the 8 hours of the study, at pH 3.0 a blow release of EM takes place during the first 4h followed by a stable controlled release. Then 5 h of incubation, the cumulative release of EM was of \sim 58%. Results observed in an acid environment (pH 3), initiate that initial blow release could be ascribed to the absorption of EM on the Se@BSA surface or owing to entrapment of EM close to the interface (Figure 5B). While a pH 7.0 the drug release pattern showed an initial blow at 4 h followed by a stable controlled release of EM with a cumulative release of \sim 16% in an incubation period of 8 h (Figure 5C). Findings indicated that at pH 7.0 cumulative release of EM was significantly slower than those in the pH.

Viability Assay of Nanoparticles in RAW 264.7 Cells

As is observed in Figure 6, the MTS assays conducted during this experiment revealed no significant differences between non-pretreated cells and pretreated cells. Even after 24 hours of incubation, the level of cell confluence remained remarkably consistent. These results suggest that exposure to Se@BSA nanoparticles and EM/Se@BSA nanoparticles at concentrations of 100 and 200 μ g/mL impact cell growth in 10 % and 15%.

J Alzheimers Dise & Rep, 2025 Volume 2(1): 8-13

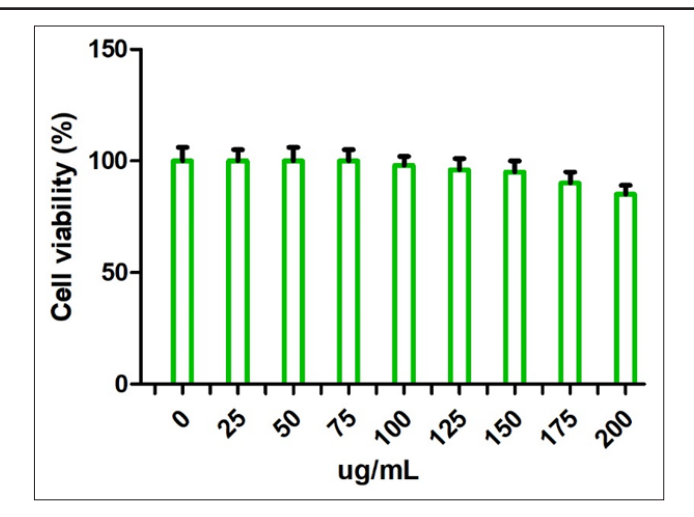


Figure 6: Viability (expressed as percentage of the control) (MTT assay) measured in control RAW 264.7 cells (0) and cells treated for 24 h with different exposure to different doses of se EM@Se (A).

Effect of EM, Se@BSA and EM/Se@BSA on Behavioral Condition in Treated AlCl, Mice

To investigate if EM, Se@BSA, and EM/Se@BSA can recover memory loss and cognitive performance, we treated AD induced-AlCl₃ mouse with EM, Se@BSA, and EM/Se@BSA for 7 weeks and carried out the T-maze test to determine spatial learning and memory deficits, exploratory and locomotor behavior was measured in an open field, and object recognition tests (Figure 7A-C).

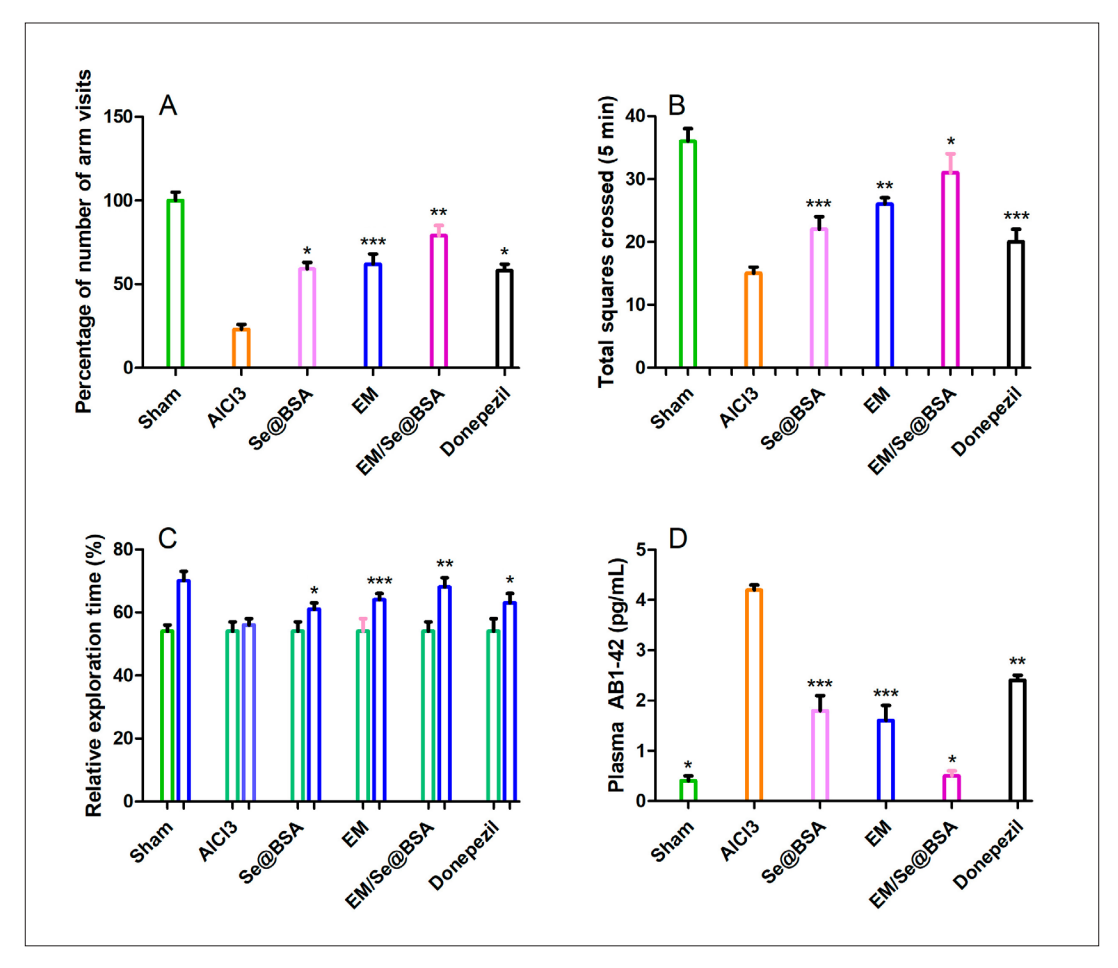


Figure 7: Effect of EM, Se NPs and EM@Se to evaluate behavioral status in experimental AD mic: Inhibition cage activity (A) T-maze tests show spatial perceptive capacity as percentage of number of arm visits for 5 min(B); total squares crossed (5 min) in open filed; In the novel object recognition test the space perceptive ability is determined as the percentage of the identification accounts a rodent in each object for 5 min (C). In the object recognition test abilities for familiar and new object are significantly different as determined by Student's t-test (D); ELISA test reducing A β deposition after EM@Se treatment in plasma of AlCl3 mice (E). Effect of samples on plasma amyloids AB1-42 (D), Data are expressed as the mean \pm SD ***p < 0.001, **p < 0.01, and *p < 0.05 compared with AlCl3 group.

J Alzheimers Dise & Rep, 2025 Volume 2(1): 9-13

Effect of EM, Se@BSA and EM/Se@BSA on Space Perceptive Ability

T-maze was utilized to investigate cognitive abilities and memory of mice in space xploration and to assess the protective effect of EM, Se@BSA, and EM/Se@BSA on com mon behavioral dysfunction in AlCl3-induced memory impairment mice. The AlCl3-induced AD (control group), the exploration rate for new routes was 28%. However, the EM, Se@BSA, and EM/Se@BSA groups exhibited higher rates of exploration for the new route, specifically, 65, 60, and 79%, respectively (Figure 7A).

Nanoparticles Enhanced Cognitive Abilities of AD Mice, in Open Field Test

In this study, mice with Alzheimer's disease (AD) induced by AlCl3 treatment were used to investigate the effects of EM, Se@BSA, and EM/Se@BSA. The AD mice exhibited a significant increase in disorderly movements without any purpose in the open field test, particularly around the central field region (as shown in Figure 7B). However, in C57BL6/J mice with AD, nanoparticles significantly improved locomotor activity compared to AlCl3-administered mice. Furthermore, the enhancement of exploration movement, memory, and cognitive abilities in the animals was well supported by results obtained from the T-maze test

Effect of EM, Se@BSA, and EM/Se@BSA on Object Recognition Ability

During the training session, the rodent did not exhibit significant recognition of two objects (A, A'). Subsequently, after 24 hours, one of the objects was replaced with two different objects (A, B). In the normal control group, there was less exploration of the familiar object compared to the novel object. However, in the Alzheimer's disease (AD) control group, curiosity toward both familiar and novel objects was observed (as shown in Figure 7C), with no statistically significant difference between the two. This lack of discrimination indicated cognitive impairment in the AlCl3-treated mice. Interestingly, animals treated with EM, Se@BSA, and EM/Se@BSA displayed improved cognitive abilities specifically related to novel objects. Notably, the EM/Se@BSA group exhibited increased curiosity about novel objects compared to the other treatment groups.

Nanoparticles Treatment Reduces Plasma Aß Deposition in C57BL6/J Mice

Given that $A\beta$ deposition is a main event in AD disease, we conducted an ELISA test to measure $A\beta$ 1-42 levels in plasma. Untreated mice exhibited higher amyloid levels compared to the control group. Treatment with nanoparticles (NPs) for 7 weeks significantly reduced insoluble $A\beta$ 1-42 deposition in AlCl3-induced AD mice, similar to the normal group (as shown in Figure 7D). In contrast, donepezil treatment reduced $A\beta$ 1-42 levels by 68% in AlCl3-mice. Our findings suggest that EM/Se@BSA treatment may improve $A\beta$ 1-42 deposition in C57BL6/J mice, achieving an 87.7% inhibition.

Effects of Nanoparticles on Hippocampal Oxidative Damage

AlCl3 treatment significantly increased lipid peroxidation (MDA) and nitrite (NO levels), reduced endogenous antioxidant enzymes, including catalase (CAT), superoxide dis- mutase (SOD), reduced glutathione (GSH), and oxidized glutathione (GSSG) levels in the hippocampus (Table 1). EM, Se@BSA, and EM/Se@BSA treatment reduce MDA levels, increase antioxidant enzymes such as CAT, SOD, oxidized glutathione, and reduced glutathione contents. Findings demonstrated that treatment of EM, Se@BSA, and EM/Se@BSA ameliorates hippocampal oxidative stress.

Table 1: The effects of EM, Se@BSA and EM/Se@BSA, on hippocampal oxidative damage including lipid Peroxidation (MDA), nitrite (NO levels), catalase (CAT), superoxide dismutase (SOD) and reduced glutathione (GSH) oxidized glutathione (GSSG) in AlCl3 treated mice.

Groups	CAT (U per mg protein)	SOD (U per mg protein)	GSH (µmol L ⁻¹)	GSSG (µmol L ⁻¹)	NO (nmol per mg protein)	MDA (nmol per mg protein)
Sham	15.28 ± 2.16	33.24 ± 4.10	99.44 ± 5.12	62.54 ± 2.90	166.32 ± 5.61	8.05 ± 2.65
Groups	CAT (U per mg protein)	SOD (U per mg protein)	GSH (μmol L-1)	GSSG (μmol L-1)	NO (nmol per mg protein)	MDA (nmol per mg protein)
AD	$8.27 \pm 1.35*$	$15.41 \pm 2.36**$	11.89 ±1.73**	93.11 ±4.65*	280.33 ±8.63*	15.78 ±3.13**
Se@BSA	10.96 ±1.01##	$22.53 \pm 3.78 \#$	77.65 ±4.06**#	$69.54 \pm 4.07 \#$	210± 6.81*	11.84 ± 2.73
EM	12.44 ± 0.99#	27.12 ±4.61##	82.57±3.88*##	67.52± 4.12#	190.77 ±7.14**	10.75 ± 2.39
EM/Se@BSA	14.35 ± 2.72#	31.76 ± 3.90##	92.34 ±6.18##	65.70 3.78##	176.33 ±9.91#	8.97 ± 1.54#
Donepezil	10.78 ±2.65##	25.97± 3.73#	70.23 ±3.15**#	72.35 ±3.62*##	225.68 ±8.53*	11.35± 3.72

The results are the means $\pm \pm SD$ (n = 5). The different asterisks (*) indicate significant differences vs ham group; (p < 0.05, *p<0.05; ** p<0.01; ***p<0.001);). The different asterisks () indicate significant differences vs Alzheimer's group; (; #p<0.01, ##p<0.05)-

J Alzheimers Dise & Rep, 2025 Volume 2(1): 10-13

Discussion

This study aimed to explore the potential neuroprotective effects of EM, Se@BSA, and EM/Se@BSA. The hypothesized mechanism of action focuses on in vitro assays and mouse odels of neurodegenerative diseases. EM was conjugated onto the surface of selenium nanoparticles (Se NPs) and characterized using various spectroscopic techniques. The synthesized Se@ BSA exhibited nano-size dimensions, high stability, an amorphous nature, and a spherical shape. Dynamic light scattering (DLS) and zeta potential analysis were employed to assess the hydrodynamic size and stability of EM/Se NPs. Zeta potential, representing the effective electric charge on NP surfaces, provided insights into particle stability. Notably, an increasing zeta potential magnitude correlated with enhanced nanoparticle stability due to electrostatic repulsion between particles. Additionally, X-ray diffraction (XRD) analysis confirmed that EM/Se@BSA exists in a pure crystalline phase. This research provides new insight into the use of nanoparticles in medicine containing selenium and phytocompounds (Baicalin and Myricetin) against protein aggregation in vitro and through a model of AD. Release of EM in gastrointestinal conditions indicates the release mode of the bioactive from the capsule material, including erosion, degradation, swelling, and dissolution. In SGF, the bioactive attached to the surface of NPs is quickly dissolved, producing a burst effect. Consequently, solution penetration into NPs leads to a determined degree of swelling in the polymer matrix, causing a dissolution-diffusion in EM in NPs, continuing with the erosion of the bloated matrix, allowing the release of the remaining EM. Meanwhile, in SI, the slow release of EM may be due to the diffusion/erosion mechanism, possibly due to the presence of both erosion and swelling simultaneously [42].

In addition, to evaluate EM/Se@BSA safest concentrations on RAW 264.7 macrophages, the nanoparticles were screened using MTT assay. The finding indicated that nanoparticles slightly affect cell viability with increasing concentrations of EM/Se@BSA, possibly to avoid accumulation inside the cells, consequently causing decreased cell death and cellular stress.

Notably, neuroprotection provided by nanoparticle treatment is linked to potent free radical scavenging properties. In our study, we investigated behavioral changes resulting from chronic aluminum exposure and evaluated the impact of nanoparticle treatment using three behavioral assays: the T-maze, open field, and object recognition tests. AlCl3-induced Alzheimer's disease mice exhibit spatial memory deficits, which were assessed in the T-maze test [43]. Compared to the control group, the AlCl3-exposed group showed significant differences. Interestingly, the EM/Se@BSA NPs group demonstrated a higher spatial exploration rate for the new route compared to both the AlCl3 group and the control group. Additionally, the EM/Se@BSA NPs group outperformed the donepezil-treated group. These findings suggest that nasal administration of EM/Se@BSA may protect against spatial memory deficits induced by AD in C57BL6/J mice. Our results show theeffect of EM/Se@BSA in the exposure of mice AD to the open field task a significant improvement in learning, and associative spatial.

In our study, nasal administration of EM/Se@BSA NPs to AD mice resulted in a heightened perception of novel objects compared to the control group. This finding supports a pronounced neuroprotective effect that improved cognitive impairment. To assess motor function, we conducted an Open Field test to determine whether nanoparticle treatment influenced mice's motor abilities. Remarkably, chronic administration of nano-

particles over 7 weeks significantly enhanced motor function in AD mice compared to untreated counterparts. This improvement was evident in the acquisition and retention of knowledge for the recommended task, demonstrating a nootropic function. Our research focused on administering EM/Se@BSA NPs to AlCl3-induced AD mice, aiming to improve AD pathology, enhance memory, and promote spatial learning, ultimately contributing to reduced plasma Aβ deposition.

Se NPs have potent antioxidants and redox properties, and the obtained results indicated that they could be promising nanoparticles for the therapy of diseases in which ox idative stress plays a critical role, such as neurological disorders [44]. Thus, Se NPs, by their powerful free radical scavenging ability, were employed as carriers to load E and M for the treatment of AD. Considering that AlCl3 treatment in mice causes oxidative damage by developing free radicals (ROS) and depleting antioxidant enzymes. In this work, we found that AlCl3 produced important oxidative damage manifested by increasing NO and MDA levels and reduced antioxidant enzymes such as CAT and SOD, as well as GSH and GSSG content. In addition, ROS generation and oxidative damage could be produced by aggregation of AB amyloid [45]. However, EM/Se@BSA treatment significantly alleviates oxidative damage in C57BL6/J mice induced by ALCl3, suggesting a neuroprotective effect against oxidative stress damage.

In this study, EM/Se@BSA can significantly alleviate oxidative stress damage in hippocampal cells, ameliorate the degeneration of hippocampal neurons, consequently improvement memory, and cognitive impairment. Efficient delivery and targeting of molecules of interest are an important challenge in AD treatments due to protective barriers of the central nervous system (blood—brain barrier (BBB)) which Is one obstacle of the accessibility of many therapeutic drug molecules. However, the nanoparticles selenium has the ability to encapsulate therapeutic EM displayed an effective drug delivery processes protecting therapeutic flavonoids deliver them to the tissues enhance their biocompatibility and toxicity and significantly alleviating AD.

Elevated plasma amyloid- β concentrations correlate with AD development. When examining plasma A β 1–42, after treatment with nanoparticles significantly reduced amyloid- β compared to untreated A β 1–42, suggesting a crucial conformational modification of the peptide indicating the neuromodulator effect of nanoparticles.

In conclusion the selenium nanoparticles were synthesized effectively through a Sol-gel synthesis route using ascorbic acid as a reducer. Synthesized nanoparticles present high stability, nano-size, amorphous nature, spherical shape, and are in pure crystalline phase. The digestion process of nanoparticles was studied in vitro simulated digestion assays; results indicated that nanoparticles were stable in simulated gastric and intestinal fluid digestion, and the formation and encapsulation of EM/Se@ BSA NPs do not affect the re lease of EM in simulated fluids. The present study provides evidence that the nanoparticles EM/Se@BSA treatment significantly avoid Aβ deposition. The neuroprotective effects of EM/Se@BSA NPs were confirmed in AlCl3-induced AD, increasing their capacity to improve cognitive functions and memory abilities as well as protect against oxidative damage. Results provide relevant insight into a new potential anti-neurodegenerative that can de- crease the severity of Aβ1-42 fibril formation. These findings showed an effective therapeutic approach in neurodegenerative disorders based on a combination of flavonoids and selenium.

Conflict of Interest

The authors have no conflict of interest in reporting.

Data Availability

Data is contained within the article.

References

- Alam P, Siddiqi K, Chturvedi SK, Khan RH (2017) Protein aggregation: from background to inhibition strategies. Intern J Biol Macromol 103: 208-219.
- Amin S, Barnett GV, Pathak JA, Roberts C, Sarangapani PS (2014) Protein aggregation, particle formation, characterization rheology. Curr. Opin. Colloid Interface 19: 438-449.
- 3. Tellone E, Galtieri A, Russo A, Ficarra S (2019) Protective effects of the caffeine against neurodegenerative diseases. Curr Med Chem 25: 5137-5151.
- 4. Marttinen M, Takalo T, Natunen R (2018) Molecular mechanisms of naptotoxicity and neuroinflammation in Alzheimer's disease front. Neurosciences 12: 963-975.
- Masters CL, Bateman R, Blennow K, Rowe CC, Sperling R (2015) Alzheimer's disease. Nat Rev Dis 1: 15056.
- Kaniakova M, Nepovimova E, Kleteckova L (2019) Combination of memantine and 6- chlorotacrine as novel multi-target compound against Alzheimer's disease. Curr Alzheimer Res 16: 821-833.
- Darvesh S, Hopkins D, Geula C (2003) Neurobiology of butyrylcholinesterase. Nat Rev Neurosci 4: 131-138.
- 8. Gao Y, Tan L, Yu JT, Tan L (2018) Tau in alzheimer's disease: mechanisms and therapeutic strategies. Curr Alzheimer Res 15: 283-300.
- 9. Congdon EE, Sigurdsson EM (2018) Tau-targeting therapies for Alzheimer disease. Nat Rev Neurol 14: 399-415.
- Wang C, Xiong M, Gratuze M, Bao X, Shi Y, et al. (2021) Selective removal of astrocytic APOE4 strongly protects against tau-mediated neurodegeneration and decreases synaptic phagocytosis by microglia. Neuron 109: 1657-1674.
- 11. Delgado JG, Saavedra MM, Miranda NM (2022) Update on brain neuroplasticity. Rev Med Sinergia 7: e829.
- 12. Chen Z, Zhong C (2014) Oxidative stress in Alzheimer's disease. Neurosci Bull 30: 271-281.
- 13. Loewen CA, Feany MB (2003) He unfolded protein response protects from tau neurotoxicity in vivo. PLoS One
- 14. Krautwald M, Leech D, Horne S (2011) The advanced glycation end product-lowering agent ALT-11 is a low affinity inhibitor of thiamine diphosphokinase. Rejuvenation Res 14: 383-391.
- Malyugina S, Skalickova S, Skladanka J, Slama P, Horky P (2021) Biogenic selenium nanoparticles in animal nutrition. A Review. Agriculture 11: 1244.
- Kang D, Lee J, Wu C, Guo X, Lee BJ, et al. (2020) The role of selenium metabolism and selenoproteins in cartilage homeostasis and arthropathies. Exp Mol Med 52: 1198-1208.
- 17. Cheng H, Huo D, Zhu C, Shen S, Wang W, et al. (2018) Combination cancer treatment through photothermally controlled release of selenous acid from gold nanocages. Biomaterials 178: 517-526.
- 18. Li J, Fu C, Feng B, Liu O, Gu J, et al. (2024) Polyacrylic Acid-coated selenium-doped carbon dots inhibit ferroptosis to alleviate chemotherapy-associated acute kidney injury. Adv Sci Weinh 11: e2400527.
- Selmani A, Ulm L, Kasemets K, Kurvet I, Erceg, I, et al. (2020) Stability and toxicity of differently coated selenium nanoparticles under model environmental exposure settings.

- Chemosphere 250: 126265.
- 20. Kalishwaralal K, Jeyabharathi S, Sundar K, Muthukumaran A (2014) A novel one-pot green synthesis of selenium nanoparticles and evaluation of its toxicity in zebrafish embryos. Artif. Cells, Nanomed Biotechnol 44: 471.
- 21. Guillin C, Vindry T, Ohlmann L, Chavatte L (2019) Selenium, Selenoproteins and Viral Infection. Nutrients 11: 2101.
- 22. Loeschner K, Hadrup N, Hansen MS, Pereira B, Gammel gaard B, et al. (2014) Absorption, distribution, metabolism and excretion of selenium following oral administration of elemental selenium nanoparticles or selenite in rats. Metal lomics 6: 330.
- 23. Rufino AT, Ramalho A Sousa A, de Oliveira JMPF, Freitas P, Gómez MAG, et al. (2021) Protective role of flavonoids against intestinal pro-inflammatory effects of silver nanoparticles. Molecules 26: 6610.
- 24. Varlamova EG, Turovsky EA, Blinova EV (2021) Therapeutic potential and main methods of obtaining selenium nanoparticles. Int J Mol Sci 22: 10808.
- 25. Kiełczykowska M, Kocot J, Paździor M, Musik I (2018) Selenium - a fascinating antioxidant of protective properties. Adv Clin Exp Med 27: 245-255.
- Calderaro A, Patanè GT, Tellone E (2022) The Neuroprotective potentiality of flavonoids on Alzheimer's disease. Int J Mol Sci 23: 14835.
- 27. Chen C, Li X, Gao P, Tu Y, Zhao M, et al. (2015) Baicalin attenuates Alzheimer- like pathological changes and memory deficits induced by amyloid beta1-42 protein. Metab Brain Dis 30: 537-544.
- 28. Zhao J, Lu S, Yu H, Duan S, Zhao J (2018) Baicalin and ginsenoside Rb1 promote the proliferation and differentiation of neural stem cells in Alzheimer's disease model rats. Brain Res 1678: 187-194.
- 29. Liu M, Guo H, Li Z (2020) Molecular level insight into the benefit of myricetin and in patients with Alzheimer's diseases. Front Aging Neurosci 12: 601603.
- 30. Liang J, López-Valdés HE, Martínez-Coria F (2014) Dihydromyricetin ameliorates behavioral deficits and reverses neuropathology of transgenic mouse models of Alzheimer's disease. Neurochem Res 39: 1171-1181.
- 31. Xia J, Guo S, Fan T (2014) Dihydromyricetin induces autophagy in HepG2 cells involved in inhibition of mTOR and regulating its upstream pathways. Food Chem Toxicol 66: 7-13.
- 32. Fish PV, Steadman D, Bayle ED, Whiting P (2019) New approaches for the treatment of Alzheimer's disease. Bioorganic. Med. Chem. 1116 Lett 29: 125-133.
- 33. Shi XD, Tian YQ, Wu JL (2021) Synthesis, characterization, and biological activity of selenium nanoparticles conjugated with polysaccharides. Crit Rev Food Sci Nutr 61: 2225-2236.
- 34. Konga H, Yang X, Zhanga Y, Fanga Y, Nishinaria K, et al. (2014) Synthesis and antioxidant properties of gum arabic-stabilizedselenium nanoparticles.
 - a. Intern J Biol Macromol 65: 55-162.
- 35. Zhu M, Zhang Y, Zhang C, Chen L, Kuang Y (2023) Rutin modified selenium nanoparticles reduce cell oxidative damage induced by H(2)O(2) by activating Nrf2/HO-1 signaling pathway. J Biomater Appl 38: 109-121.
- Anand V, Ksh V, Kar A, Varghese E, Vasudev S, et al. (2024) Encapsulation efficiency and fatty acid analysis of chia seed oil microencapsulated by freeze-drying using combinations of wall material. Food Chem 430: 136960.
- Jiang H, Wang R, Zhoum F, Wu Y, Li S, et al. (2022) Preparation, physicochemical caracterization, and cytotoxicity of selenium nanoparticles stabilized by Oudemansiella

J Alzheimers Dise & Rep, 2025 Volume 2(1): 12-13

- raphanipies polysaccharide. Int J Biol Macromol 211: 35-46.
- 38. Dong L, Xie HZ, Jia L, Hong L, Li G (2023) Inhibition of amyloid β aggregation and cytotoxicity by berbamine hydrochloride. Chemistry 29: e202301865.
- 39. Pang QQ, Kim J, Choi JM, Song J, Lee S, et al. (2022) Cirsium japonicum var. Maackii improves cognitive impairment under amyloid Beta 25-35-Induced Alzheimer's disease model. BioMed Res Intern 1-11.
- 40. Sturman O, Germain PL (2018) Bohacek exploratory rearing: a context- and stress-sensitive behavior recorded in the open-field test. J Stress 21: 443-452.
- Mostafa NM, Mostafa AM, Ashour ML, Elhady SS (2021) Neuroprotective Effects of Black Pepper Cold-Pressed Oil on Scopolamine-Induced Oxidative Stress and Memory Impairment in Rats. Antioxidants (Basel) 10.
- 42. Pola CC, Moraes RF, Medeiros AA, Teofilo RF, Soares FF, et al. (2019) Development and optimization of pH-responsive PLGA-chitosan nanoparticles for triggered release of antimicrobials. Food Chem 295: 671-679.
- 43. Zatta P, Tamas K, Mario S, Guy B (2002) Aluminium (III) as a promoter of cellular oxidation. Coord Chem Rev 228: 271-284.
- 44. Kiełczykowska M, Kocot J, Paździor M, Musik I (2018) Selenium a fascinating antioxidant of protective properties. Adv Clin Exp Med 27: 245-255.
- 45. Belkacemi A, Ramassamym C (2012) Time sequence of oxidative stress in the brain from transgenic mouse models of Alzheimer's disease related to the amyloid-beta cascade. Free Radic Biol Med 52: 593-600.

Copyright: ©2025 Rosa Martha Pérez Gutiérrez, et al. This is an open-access article distributed under the terms of the Creative Commons Attribution License, which permits unrestricted use, distribution, and reproduction in any medium, provided the original author and source are credited.

J Alzheimers Dise & Rep, 2025 Volume 2(1): 13-13